Supplementary material for: Shortening and structural architecture of the Andean fold-thrust belt of southern Bolivia (21°S): Implications for kinematic development and crustal thickening of the central Andes

SECTION SM1: BALANCED CROSS SECTION METHODS

The balanced cross section was constructed based on field data projected from east-west mapping traverses, which are oriented perpendicular to the regional strike of thrust faults and folds (Plate 2). Because field data could not be collected in an uninterrupted east-west transect, map data were projected from six across-strike traverse segments. Each segment contains a high density of field measurements, and segment breaks were placed at stratigraphic or structural contacts that are continuous along strike (Plate 1). On Plate 2, the deformed and corresponding restored cross sections are both displayed at 1:200,000-scale.

The deformed and restored sections were hand-drafted simultaneously, by matching line lengths of individual thrust sheets and maintaining unit thicknesses (e.g., Dahlstrom, 1969; Elliott, 1983). The manner in which the space above the basal décollement of the thrust belt is filled was constrained by all available geometric and stratigraphic data, as well as published geophysical constraints (e.g., Woodward et al., 1989; McQuarrie et al., 2008b). To a first-order, viability of the cross section is established by conserving slip across the thrust belt and balancing basement shortening with upper crustal shortening (McQuarrie, 2002; McQuarrie et al., 2005; McQuarrie et al., 2008b). The final line-length balanced section was compared to an area balanced cross section (Section SM5) to ensure that shortening estimates were reliable.

Published seismic reflection data and well logs constrain the subsurface geometry and stratigraphic thicknesses at the eastern and western boundaries of the cross section, defining an average dip of 1-2º W for the basal décollement at the eastern Andean thrust front in the Chaco Plain (Baby et al., 1992; Dunn et al., 1995; Uba et al., 2009), and revealing a ~6 km structural step at the EC-Altiplano boundary (Elger et al., 2005) (Plate 2). The near-surface geometry and across-strike thickness variations of sedimentary rock units were obtained using apparent dips calculated from our mapping. The non-uniqueness of the cross section geometry increases with structural depth because the manner in which rocks are deformed to fill space is unknown without dense coverage of seismic data or direct observations (e.g., Woodward et al., 1989; McQuarrie et al., 2008b). However, because stratigraphic divisions and regional thickness variations are well established in Bolivia, the geometric ambiguity is reduced as long as thicknesses are honored and the shortening recognized at the surface is balanced at depth by kinematically-viable structures (e.g., McQuarrie et al., 2008b).

The geometries of subsurface faults were constructed using basic models for fault bend folds (Suppe, 1983) and fault propagation folds (Mitra, 1990; Suppe and Medwedeff, 1990). The orientations of fold axial planes were determined by bisecting the interlimb angle at fold hinges, and most axial planes were modeled as kink surfaces (e.g., Suppe, 1983). Areas of the cross section were divided into dip domains, based on the average apparent dips of attitude measurements, and dividing lines between adjacent dip domains were treated as kink surfaces. Regional changes in exposure level and structural elevation require major subsurface features at depth such as footwall and hanging wall ramps (e.g., Kley et al., 1996; McQuarrie, 2002). Deep seismic reflection data (Allmendinger and Zapata, 2000) and gravimetric models (Kley et al., 1996) provide additional insights into the basement architecture, and constrain the location of major ramps. Teleseismic data (Wigger et al., 1994; Schmitz and Kley, 1997; Yuan et al., 2000; Baumont et al., 2002; Beck and Zandt, 2002) provide the first-order crustal architecture and depth to the basement-cover contact in the interior of the thrust belt (e.g., McQuarrie, 2002; McQuarrie et al., 2005). Late Cretaceous shallow marine strata in the EC and Altiplano and time equivalent silcretes developed in Cretaceous rocks of the SAZ (Sempere 1994; Sempere et al., 1997) are used as a correlative surface across the full width of the transect, in order to restore the undeformed cross section to paleohorizontal (Fig. 2; e.g., Kley, 1996). This horizontal datum highlights the inherited structural geometry prior to Cenozoic shortening.

Although the largest contributor to total shortening errors in balanced cross sections results from stratigraphic uncertainties (Table SM2; Judge and Allmendinger, 2011; Allmendinger and Judge, 2013), we used conservative geometries that minimize shortening in all cases by drafting eroded hanging wall cutoffs just above the erosion surface, unless subsurface data necessitated otherwise. Three-dimensional finite strain analysis from the central Andes indicates that internal strain within individual thrust sheets did not contribute significantly to cumulative Andean shortening (Eichelberger and McQuarrie, 2014), and that 2-D cross sections are therefore an accurate representation of total plane-strain shortening across the thrust belt. Detailed justifications for individual drafting decisions on the cross section are annotated on Plate 2 and detailed discussion of shortening uncertainty can be found in section SM5.

SECTION SM2: STRUCTURAL REINTERPRETATION OF THE TUPIZA REGION

The structural and sedimentological history of Cenozoic basins in the Tupiza region have been studied in detail by several authors (Hérail et al., 1996; Kley et al., 1997; Horton, 1998; Müller et al., 2002), yet the interpreted kinematics (dominantly E- vs. W-vergent) and style of thrusting (thin vs. thick skinned) are conflicting due to disputed structural-stratigraphic relations between the Cenozoic basins and adjacent Ordovician rocks, and debate over reactivation of Cretaceous rift structures (Sempere, 2000; Horton, 2000). Consequently, shortening in the Tupiza region was simply assumed to be 40% based on shortening magnitudes reported from adjacent thrust belt segments to the east and west. However, published cross sections through the Tupiza region are not actually balanced (Müller et al., 2002), leaving the kinematic viability of the EC as a whole in question. Therefore, disputed field relationships (e.g., Sempere, 2000; Horton, 2000) were reexamined to resolve contradictory interpretations in order to construct a balanced cross section that is viable and compatible with the geometry and kinematics of the thrust belt segments adjacent to the Tupiza region (Plate 2).

The easternmost basin, the Nazareno basin, is an asymmetric syncline that thickens westward toward the more steeply dipping western limb. The eastern margin of the Nazareno basin has been mapped as a W-vergent thrust fault that places Ordovician rocks over the Miocene Nazareno Formation (Servicio Geologica de Bolivia, 1992; Kley et al., 1997; Müller et al., 2002), and as a stratigraphic contact (Horton, 1998). Upon reexamination in the field, we interpret this contact as a gently W-dipping angular (~15-40°) unconformity (Fig. SM1B, Plate 1). In addition, thrust faults along the eastern margin of the Nazareno basin are E-vergent, placing Ordovician rocks over thin sections of W-dipping Nazareno Formation (Fig. SM1C). No obvious thrust faults are observed along the western flank of the basin (Fig. SM2), and we map the western margin as a stratigraphic contact, with the basal early Oligocene(?) Nazareno conglomerate overlying Middle Ordovician rocks across a ~60° angular unconformity (Fig.

SM3). Although there is no basin-bounding fault, a progressive upsection decrease in bedding dips observed in early Oligocene(?) to middle Miocene rocks within the western limb of the basin suggests syn-deformational deposition.

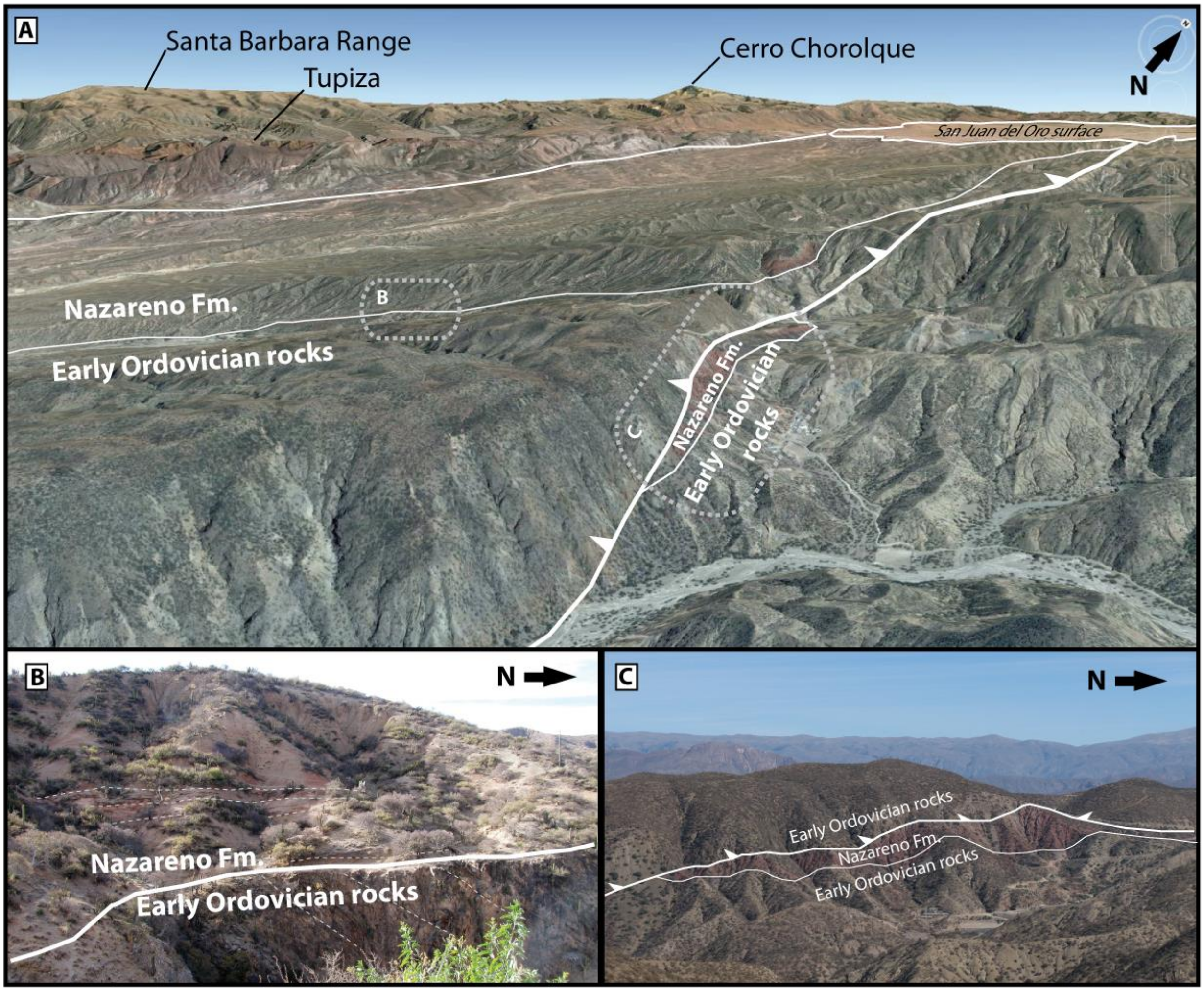

Figure SM1. Annotated field relationships along the eastern margin of the Nazareno Basin. A: Oblique GoogleEarth view looking northwest; gray dashed boxes show locations of annotated photos in B and C. B. Middle Miocene Nazareno Formation in angular unconformity above Early Ordovician rocks along the eastern margin of the Nazareno basin. C. Early Ordovician rocks thrust eastward over middle Miocene Nazareno Formation ~3 km east of the eastern Nazareno basin margin.

The region between the Nazareno basin and the Eastern Tupiza Basin is characterized by Ordovician and Mesozoic rocks that are tightly to isoclinally folded into an anticline-syncline pair (Fig. SM2). The tight folds are overlapped by Oligocene volcanic rocks that are folded into an open anticline

(Fig. SM2). The tight synclinal folding of these Mesozoic rocks has been attributed to an E-vergent footwall breakthrough of an inverted Jurassic normal fault at the Mesozoic-Ordovician contact in the eastern limb of the syncline (Kley et al., 1997; Sempere, 2000; Müller et al., 2002), but as other authors noted (e.g., Hérail et al., 1996; Horton, 1998, 2000), no obvious fault could be located along the eastern edge of the syncline. New structural measurements suggest that the contact is depositional, as the Mesozoic rocks in both limbs of the syncline dip concordantly with underlying Ordovician rocks (Fig. SM2, Plate 1), and the stratigraphic order of Mesozoic rocks in both limbs is the same (Sempere, 2000). We propose that an inverted Jurassic normal fault may be present, but if so, it is concealed beneath the western edge of the Nazareno basin, and only accommodated minor inversion (Fig. SM2).

The Eastern Tupiza basin is a N-trending, isoclinally folded syncline, bound on the east by the W-vergent Jurcuma thrust and on the west by the E-Vergent Seca thrust (Fig. SM2). In the internal part of the basin, the oldest Cenozoic strata (Bella Vista conglomerate, Fig. 2) were cut by a W-vergent fault (Bella Vista thrust), but overlapped by Tupiza Formation volcanics (Horton, 1998). The Central Tupiza basin is also a N-trending, isoclinally folded syncline, but is reinterpreted to be contained within a synformal klippe whose limbs were thrust over the adjacent Western and Eastern Tupiza basins across the Palala and Seca thrusts (respectively). The Palala thrust is defined by a steep escarpment that separates Middle Ordovician rocks from Miocene rocks in the Western Tupiza basin, along which Middle Ordovician rocks were thrust westward over the top of Cenozoic rocks of the Western Tupiza basin (Fig. SM4). Conversely, Middle-Ordovician rocks along the Seca thrust are observed to be thrust eastward over the late Oligocene to Miocene rocks in the adjacent Eastern Tupiza basin (Fig. SM4). Bedding measurements on the western limb of the Central Tupiza basin show that Ordovician strata and early Miocene Tupiza Formation conglomerates dip concordantly to the east (~55°), suggesting a stratigraphic contact between the two (Fig. SM2, Plate 1). Measured sections show that the Tupiza Formation conglomerates in the Central Tupiza basin lack growth strata (Horton, 1998). In contrast, an upsection decrease in bedding dips is observed within the Tupiza Formation conglomerate along the western margin of the Eastern Tupiza basin (Horton, 1998).

Late Oligocene- middle Miocene rocks in the Western Tupiza basin define an asymmetric syncline that thickens and steepens toward the footwall of the basin-bounding Palala thrust (Fig. SM2). Along the eastern margin of the basin, early to middle Miocene rocks display a footwall growth relationship, as they exhibit a progressive upsection decrease in bedding dip (Horton, 1998). The western margin of the basin is interpreted as a stratigraphic contact as field observations, the nature of the mapped contact, and bedding measurements show that the middle Miocene rocks onlap onto Late Ordovician rocks across an unconformity with minimal angularity, and both the Miocene and Late Ordovician rocks dip gently to the east (Fig. SM4). The structural-stratigraphic relationship is more complex along the southwestern flank of the basin, where tightly folded late Oligocene- early Miocene rocks (Huerto Waykho conglomerate, Palquiza unit, Chifloca unit) are separated from early Oligocene conglomerates (Urulica conglomerate) by a narrow strip of Ordovician rocks (Plate 1). Reexamination of this relationship shows that the narrow strip of Ordovician rocks are steeply east dipping, and thrust westward over the top of the Urulica conglomerate (Plate 1, Figs. SM2, SM4). The W-vergent thrust dies out along strike to the north and south, and the contact between Ordovician and late Oligocene rocks in the hanging wall of the thrust is interpreted as a stratigraphic contact.

The Santa Barbara Range is a broad antiformal range of Ordovician rocks that lies between the Western Tupiza basin the Estarca basin (Fig. SM2). A steep escarpment (heretofore named the Santa Barbara thrust) defines the boundary between the Santa Barbara Range and the Estarca basin, and field observations confirm that Late Ordovician rocks were thrust westward over the top of Neogene rocks along the escarpment (Fig. SM5). The Estarca Basin was folded into an open syncline, and the Neogene Estarca Formation thickens and coarsens toward the basin-bounding Santa Barbara thrust along the eastern margin of the basin (Horton, 1998). The western margin of the basin tapers gently to the west where it onlaps onto the underlying, and more tightly folded Ordovician rocks, and is overlapped by the late Miocene erosion surface (Müller et al., 2002).

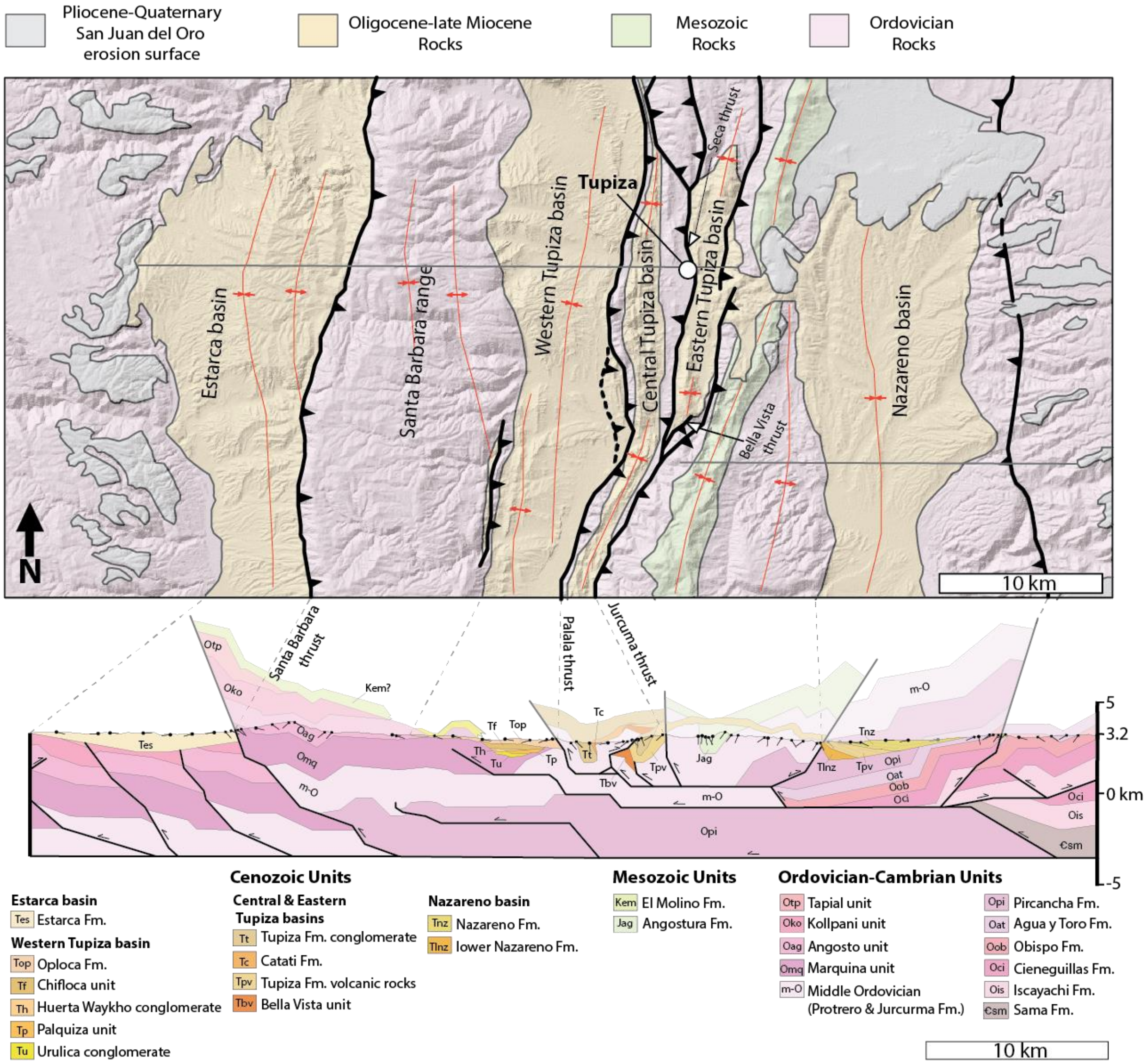

Figure SM2. Simplified geologic map of the western Cenozoic outcrop belt (Tupiza region) within the Eastern Cordillera (modified from Horton, 1998) with a geologic cross section shown below. Tie lines connect important structures and contacts shown on the map. Scale for the map and cross section differ.

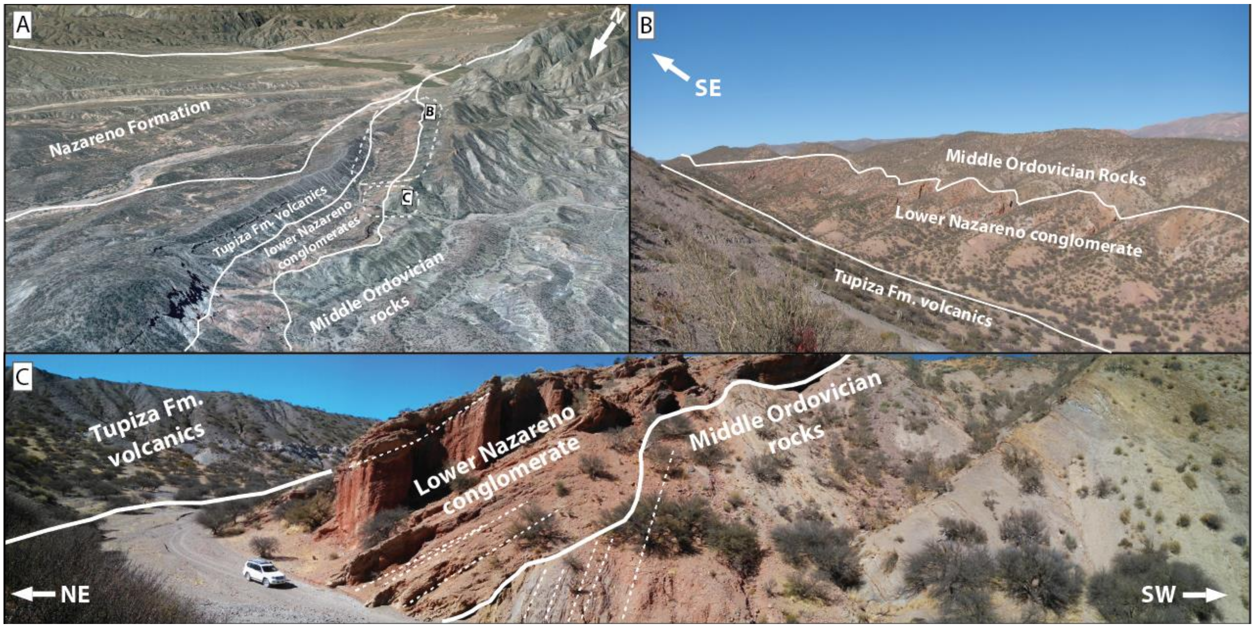

Figure SM3. Annotated field relationships along the western margin of the Nazareno basin. A. Oblique GoogleEarth view looking southeast at east-dipping Cenozoic units of the Nazareno basin. Dashed boxes show locations of annotated photos in B and C. B. Southwest facing view of an east-dipping dip-slope of the basal Lower Nazareno conglomerate overlying Middle Ordovician rocks across a depositional contact. C. Southeast-facing view of the angular unconformity (60° dip difference) between basal Lower Nazareno conglomerate and underlying Middle Ordovician rocks.

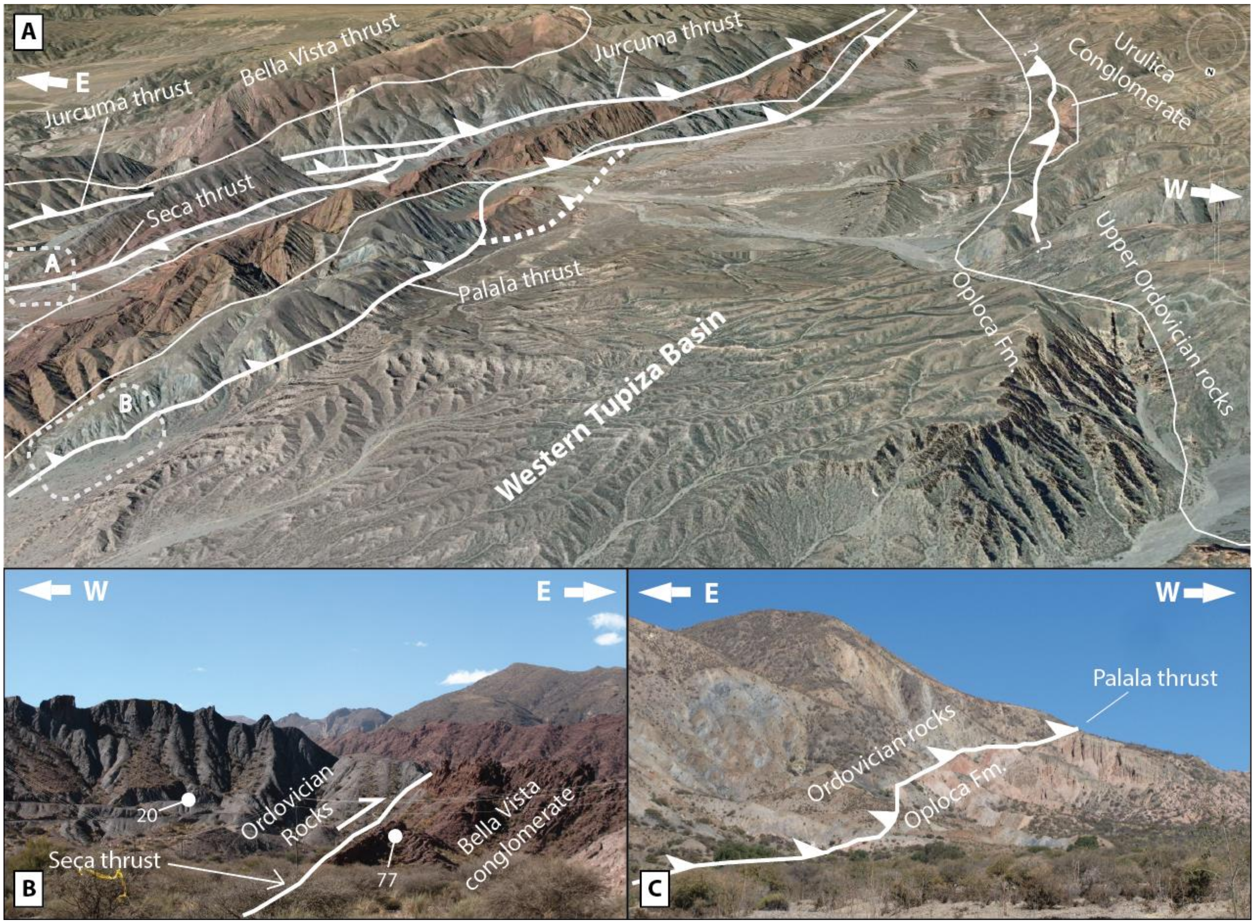

Figure SM4. Annotated field relationships of the Western Tupiza basin and parts of the Central and Eastern Tupiza basins. A. Oblique GoogleEarth view looking southeast. Heavier lines represent faults, with thinner lines showing stratigraphic contacts between Cenozoic, Mesozoic, and Ordovician rocks. Note only stratigraphy is labeled along the western edge of the Western Tupiza basin. Dashed boxes show locations of annotated photos in B and C. B. Looking Facing north at the southwestern margin of the Eastern Tupiza basin. Ordovician rocks are thrust eastward over the Bella Vista conglomerate of the Eastern Tupiza basin. C. Looking Facing south at the escarpment along western margin of the Central Tupiza basin. East dipping Ordovician rocks are thrust westward over east-dipping middle Miocene Oploca formation in the Western Tupiza basin.

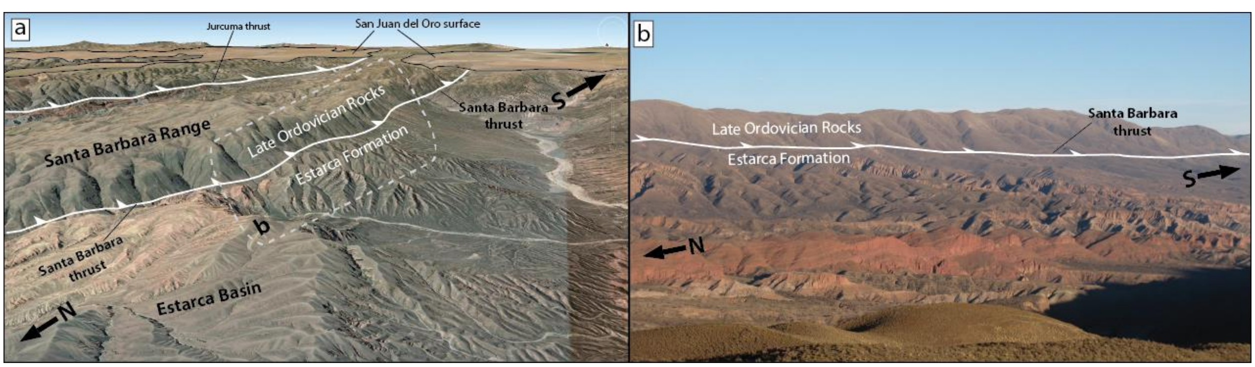

Figure SM5. Annotated field relationships of the Estarca basin. A. Oblique GoogleEarth view looking southeast. A steep escarpment defines the eastern margin of the Estarca basin (Santa Barbara thrust), with Ordovician rocks thrust westward over the middle Miocene Estarca formation. B. Photo looking east from the western edge of the Estarca basin, showing the thrust relationship described above.

SECTION SM3: SEQUENTIAL RESTORATION OF THE TUPIZA REGION

The new cross section of the Tupiza region is restored sequentially (Fig. SM6), in order to demonstrate that it is compatible with measured paleocurrent indicators, clast provenance and composition, facies relationships, growth strata, and isotopic age data within the Oligocene to late-Miocene basins, and to quantify shortening through time. Early exhumation and erosion in the EC stripped away ~2.5-3 km of Mesozoic rocks and Cenozoic foredeep deposits in the Tupiza region between 40-32 Ma (Ege et al., 2007). Following this, coarse-grained sedimentary deposits accumulated within localized basins in the western Cenozoic outcrop belt adjacent to active contractional structures (Hérail et al., 1996; Tawackoli et al., 1996; Horton, 1998, 2005). Isotopic age constraints for the oldest strata deposited within the Tupiza region basins are not available (Fig. 2, e.g., Urulica, Bella Vista, and possibly the lower Nazareno conglomerates), but postdate 40-36 Ma removal of earlier Cenozoic foredeep deposits, and predate the overlapping ~29-20 Ma Tupiza Formation volcanics (Hérail et al., 1996; Tawackoli et al., 1996). An apatite fission track (AFT) cooling age obtained from Mesozoic basalt between the Eastern Tupiza and Nazareno basins suggests activity on early thrusts in the Tupiza region at approximately ~32 Ma (Tawackoli et al., 1996) were in sequence with westward migration of deformation across the backthrust belt from ~40-27 Ma (Ege et al., 2007). AFT ages from Ordovician strata in the Estarca basin (Ege et al., 2007; Fig. SM5b) mark the beginning of out of sequence deformation in the western EC that lasted from ~26 Ma to no later than ~10 Ma. The presumed pre-exhumational geometry of the thrust belt (~40 Ma) is shown in Plate 2, and the sequential restoration begins after ~32 Ma (Fig SM6a). The San Juan del Oro surface overlaps structures and rocks (e.g., Fig. SM5a) in the Tupiza region and is undeformed, suggesting the present day configuration (Fig. SM6e) was attained by ~10 Ma (Gubbels et al., 1993). Detailed shortening rates on individual faults were not available with the given data; therefore, each sequential section depicts the amount of shortening that was likely accomplished within a particular time frame, as dictated by isotopic ages in synorogenic sediments in adjacent basins. However, each individual sequence may slightly over- or underestimate the amount of shortening between time frames because it is impossible to know the exact timing of fault activity unless it is overlapped by a dateable surface or sequence.

Deposition of the Urulica, Bella Vista, and lower Nazareno conglomerates record the first phase of proximal active folding and thrusting (Fig. SM6b-c). Paleocurrent data show that the Bella Vista conglomerate was sourced from both the west and east (Horton, 1998). The eastern source was likely related to activity on the proximal W-vergent Bella Vista and Jurcuma thrusts as the Bella Vista conglomerate is folded into an asymmetric syncline in the footwall of the Bella Vista thrust (Horton, 1998). A topographic high is interpreted to the west as a likely source of westerly derived sediments (Fig. SM6b-c). Along the western limb of the Nazareno basin, progressive upsection decrease of dips in Tertiary rocks, eastward flowing paleocurrent data (Horton, 1998), and the lack of a basin bounding fault indicate that the basin developed on the flank of a growing fold to the west. Isotopic age data suggest deposition of the basal conglomerates in the Nazareno basin and growth of the adjacent fold initiated before ~21 Ma (Hérail et al., 1996; Tawackoli et al., 1996). In the sequentially restored cross section (Fig. SM6b-c), activity on the Bella Vista and Jurcuma thrusts, early synclinal folding of the Mesozoic and underlying Ordovician rocks between the Eastern Tupiza and Nazareno basins, and growth of the fold on the western flank of the Nazareno basin are kinematically linked. As slip is fed westward to the Bella Vista and Jurcuma thrusts via a ramp that cuts up from the base of the Paleozoic section to the secondary décollement at the base of the Middle Ordovician rocks, the fold on the flank of the Nazareno basin and the syncline cored by Mesozoic rocks are subsequently developed by fault bend folding. The deformation associated with deposition of the Urulica conglomerate is less clear, as there are no paleocurrent indicators. Minor fault propagation folding and fault bend folding due to west-directed slip on the décollement at the base of the Paleozoic section is inferred in order to generate minor topography that partitioned the Western Tupiza basin from the early Central and Eastern Tupiza basins as indicated by differing clast compositions of the two basins (Fig. SM6b, Horton, 1998).

During the late-Oligocene to early-Miocene (~26 to 20.9 Ma, Fig. SM6c-d) growth strata are lacking and sedimentary deposits are dominated by a fine grained fluvio-lacustrine facies (Horton, 1998). Furthermore, the Tupiza formation volcanic deposits overlap folded Mesozoic and Ordovician rocks between the Nazareno and Eastern Tupiza basins, and overlaps the Bella Vista and Jurcuma thrusts (Horton, 1998). However, minor deformation is inferred to explain partitioning of the Eastern, Central, and Western Tupiza basins as sediments deposited during this time period were confined to separate basins (Figure 2). Although minor in total magnitude, continued slip fed over the footwall ramp at the western edge of the Nazareno basin into the flat in Middle Ordovician rocks resulted in progressive limb rotation and angularity between the basal Nazareno conglomerates and the overlying Tupiza formation volcanics along the western flank of the Nazareno basin (Fig. SM6c-d).

The early to middle Miocene (~20.9 to 15.7 Ma) was marked by an increase in sediment accumulation and fault activity (Fig. SM6e). Isotopic age data indicate that the onset of deposition of the Tupiza formation conglomerates in the Central and Eastern Tupiza basins began after 20.9 Ma but was fully underway by 17.6 Ma (Hérail et al., 1996; Tawackoli et al., 1996), and that deposition of the Estarca formation in the Estarca basin began by 16.7 Ma (Müller et al., 2002). Interconnection between the Central and Eastern Tupiza basins is indicated by deposition of the Tupiza formation conglomerate across both basins. Growth structures along the western margin of the Eastern Tupiza basin suggest that activity on the Seca thrust initiated during this period (Horton, 1998). However, shortening was either minimal or the sedimentation rate outpaced any topography generated by fault activity because the Central and Eastern Tupiza basins apparently remained interconnected. The Tupiza Formation conglomerate was derived from the west, and records an unroofing sequence in which Ordovician clasts increase upsection at the expense of distinct clasts of Late Cretaceous stromatolitic detritus (Horton, 1998). However, in the Estarca basin, paleocurrent data show westward flow with clasts composed entirely of Ordovician rocks (Horton, 1998). These data are interpreted to mark the growth of the Santa Barbara Range and initiation of the W-vergent Santa Barbara thrust on the eastern flank of the Estarca Basin. The thrust ramps up from the base of the Paleozoic section to the surface, and the Santa Barbara Range is deformed by fault-bend folding (Fig. SM6e). During incipient fault activity, Cretaceous rocks were eroded from the Santa Barbara Range, and detritus was transported eastward into the Central and Eastern Tupiza basins, apparently bypassing the Western Tupiza basin. With continued growth of the range, material was shed both to the west (Estarca basin) and east (Central and Eastern Tupiza basins), but only after the majority of Late Cretaceous rocks were unroofed. The E-vergent fault on the eastern margin of the Nazareno basin accommodated some shortening prior to deposition of a ~12.79 Ma tuff in the upper part of the Nazareno formation (Gubbels et al., 1993) because the Nazareno Formation is deposited in an angular unconformity with the underlying Ordovician rocks along the eastern margin of the basin. We show this early shortening taking place between ~20.9 and 15.7 Ma, but it may have taken place earlier (Fig SM6e).

The final and most significant phase of deformation occurred between ~15.7 and 10 Ma, and accounts for ~56% of the total out of sequence shortening (Fig. SM6f). Growth strata along the eastern flank of the Western Tupiza basin and axial transport to the southeast due to resultant growth of topography indicate that deposition of the ~15.7 Ma Oploca Formation was synchronous with activity on the W-vergent Palala thrust (Horton, 1998). The Tupiza Formation conglomerate conformably overlies Middle Ordovician rocks, there are no recorded growth relationships in the Tupiza Formation conglomerates in the Central Tupiza basin, and the Palala thrust cuts the youngest Tupiza Formation conglomerate. Therefore, activity on the Palala thrust postdates deposition of the Tupiza Formation conglomerate (Horton, 1998). The Central and Eastern Tupiza basins became totally partitioned by activity on the E-vergent Seca thrust. The Palala and Seca thrusts are detached from a flat in the middle part of the Middle Ordovician section (Fig. SM6f), and a fault propagation fold kinks the eastern limb of the Central Tupiza basin, resulting in vertical to overturned and isoclinal tightening of the Central Tupiza basin. The W-vergent Jurcuma thrust is partially reactivated and cuts the Tupiza Formation volcanics and conglomerate. As continued slip was fed westward over the footwall ramp below the Nazareno basin, up to the detachment levels of the Palala, Seca, and Jurcuma thrusts, the syncline of Mesozoic rocks between the Eastern Tupiza and Nazareno basins became more tightly folded, whereas the overlying Tupiza Formation volcanics were folded into an open antiform (Fig. SM6f). Similarly, the Nazareno Formation, which is dated at ~12.79 Ma in the upper part of the section (Gubbels et al., 1993), was deposited in angular unconformity with the earlier deposited Tupiza Formation volcanics, due to progressive limb rotation as slip was fed westward and the Nazareno basin passed over the footwall ramp. The final increment of shortening occurred on the eastern flank of the Nazareno basin, where Ordovician rocks are thrust eastward over a narrow sliver of the Nazareno Formation (Fig. 3). The undeformed, ~10 Ma San Juan del Oro erosion surface overlaps the entire Tupiza region, providing a minimum constraint on cessation of significant deformation and shortening across the EC (Gubbels et al., 1993).

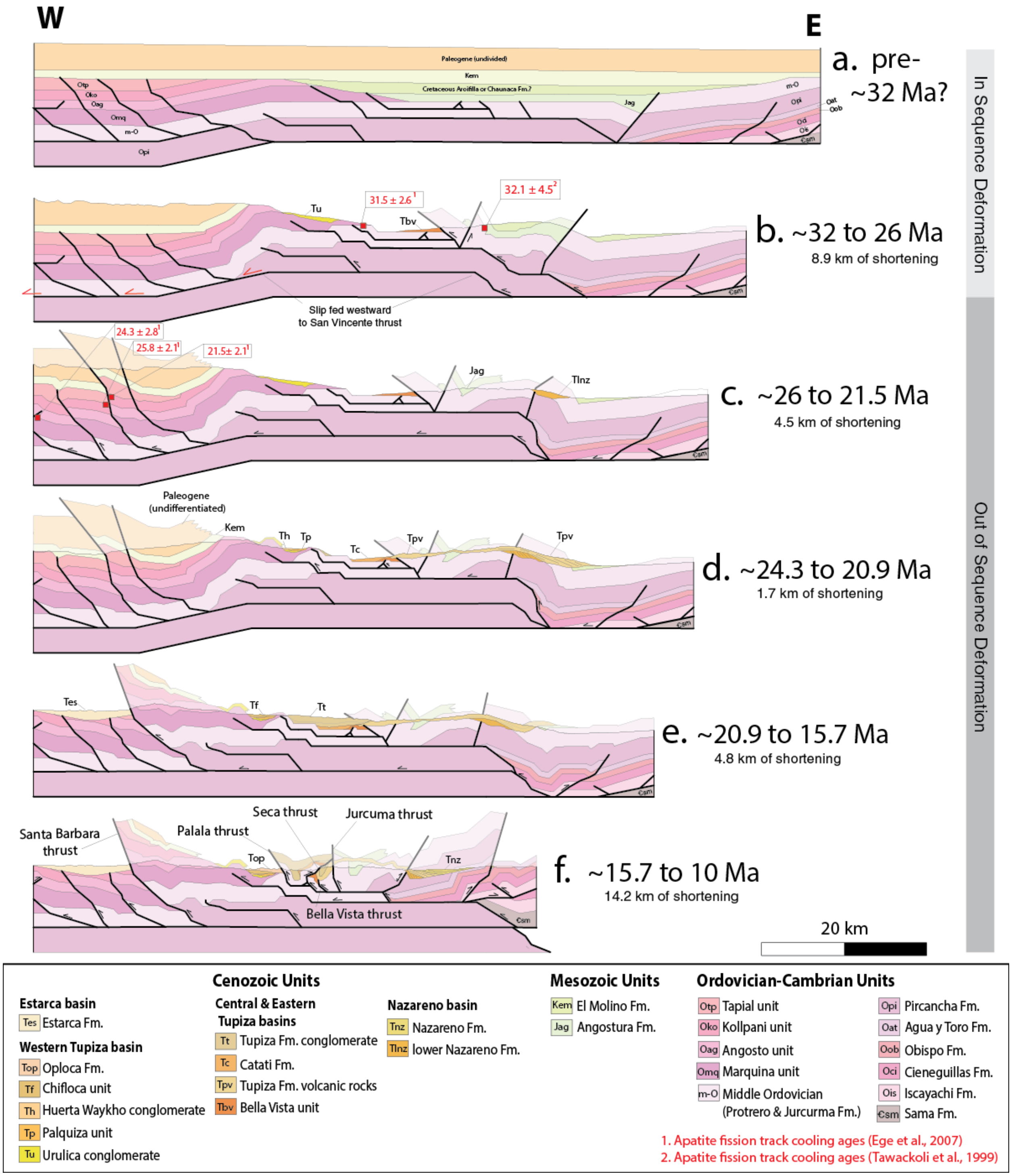

Figure SM6. ~32-10 Ma sequential restoration of the Tupiza region based on the new mapping and cross section, coupled with facies analysis, paleocurrent data, and clast provenance data from Horton (1998). Units shown on the cross section are listed; see Figure 2 and Plate 1 for unit correlation charts. A. Pre ~32 Ma thrust belt configuration prior to proximal deformation and intermontane sedimentation. B. Fault activity focused on the Jurcuma and Bella Vista thrusts is synchronous with deposition of Urulica, Bella Vista, and possibly the lower Nazareno conglomerate. C. Apatite fission-track cooling ages (Ege et al., 2007) mark onset of out of sequence deformation focused deformation west of the Santa Barbara Range D. Lull in shortening activity, deposition of fine grained fluvio-lacustrine deposits (Huerta Waykho, Palquiza, Catati units) in the Western and Central Tupiza basins, and overlap of volcanic units on formerly active thrusts in the Eastern Tupiza and Nazareno basins. E. Major fault activity is focused on the Santa Barbara thrust, which was the principal source of sediment for the Estarca Formation and Tupiza fFormation conglomerate. F. Fault activity is focused on the Palala, Seca, and reactivated Jurcuma thrusts as the Oploca and Nazareno formations are deposited in the Western Tupiza and Nazareno basins (respectively). The ~10 Ma undeformed San Juan del Oro erosion surface marks cessation of significant deformation in the EC.

SECTION SM4: UNCERTAINTIES OF THE BALANCED CROSS SECTION

Uncertainties of the line length-balanced cross section across the retroarc thrust belt (Plate 2) are assessed by constructing an area-balanced cross section and formally propagating errors using the program AreaErrorProp (e.g., Judge and Allmendinger, 2011). Assuming that the modern cross sectional area is equal to the area of the undeformed stratigraphic section, area balance shortening estimates are determined by tracing an enveloping polygon that encompasses the pre-deformational area of the deformed, line length balanced cross section, and by describing the initial area as a polygon defined by the stratigraphic thicknesses at each end (Figs. SM7-8; Mitra and Namson, 1989; Judge and Allmendinger, 2011). Because the areas of both the initial and deformed state of the cross section can be calculated analytically, errors can be propagated formally. Horizontal shortening errors are quantified by assigning uncertainty to individual vertexes of the enveloping polygon (Figs. SM7-8) and defining them as eroded hanging wall, subsurface stratigraphic, depth to decollement uncertainties, and stratigraphic uncertainties for the undeformed initial wedge (Judge and Allmendinger, 2011). Gaussian distribution of error is assumed (i.e., errors are random and uncorrelated).

The line length-balanced cross section across the central Andes shows that the initial undeformed wedge has a non-constant taper (Plate 2); however, the program AreaErrorProp assumes a simple initial wedge of uniform taper, which will always yield less shortening if the initial wedge has a non-uniform taper (Allmendinger and Judge, 2013). In order to account for the shortening deficit that results from this problem, we follow the iterative process outlined by Allmendinger and Judge (2013):

1) The enveloping polygon of the deformed section is traced, error is assigned to individual vertices, stratigraphic thicknesses and uncertainties are defined for the left and right ends of the undeformed area, and shortening is calculated by returning the area of the deformed cross section to a wedge of initial uniform taper.
2) The non-uniform wedge based on the line length balanced section (Plate 2) is traced, assigning the same stratigraphic thicknesses at the left and right ends as were assigned to the undeformed, uniformly tapered wedge in step 1.
3) Uncertainties were assigned to vertices where the taper in the traced polygon from step 2 change. We followed the recommendation of assigning a ±5 km horizontal uncertainty (Allmendinger and Judge, 2013), but assign a vertical uncertainty that is equal to 12-15% of stratigraphic thickness of the undeformed wedge.
4) Run the area balance and error propagation again in AreaErrorProp, restoring the non-uniform tapered wedge to a uniformly tapered wedge as in step 1. Non-uniform wedges that are convex up will return a negative shortening value.
5) Subtract the total shortening from step 4 from the shortening calculated in step 1 to determine the total shortening.
6) The total uncertainty is determined by taking the square root of the sum of the squares of the error in step 1 and 4.

Figures SM7 and SM9 graphically illustrate this iterative process. In Figures SM7 and SM9, and Tables SM2 and SM3, iteration 1 refers to step one in the process outlined above, and iteration 2 refers to steps two through four in the process outlined above.

Vertices were differentiated based on type (i.e., decollement, normal subsurface, surface, and eroded hanging wall) and assigned error based on our assumptions (i.e., minimum slip on eroded hanging walls) and geologic insight (i.e., geologic mapping, well data, geophysical data). In the Chaco Plain, the subsurface structure and stratigraphic architecture of the upper ~7 km of the crust is well established from seismic reflection data tied to well logs, and it has long been recognized that that the basal décollement in the Chaco Plain, SAZ, and IAZ is located at the base of the Silurian section (Baby et al., 1992; Dunn et al., 1995). In the Chaco Plain the thickness of Silurian and lower Devonian rocks is poorly constrained because oil wells do not penetrate below their base (Baby et al., 1992; McQuarrie, 2002). However, the full thickness of the Devonian section is exposed extensively across the IAZ and the base of the Silurian is only exposed along the western edge of the IAZ. Accordingly, the depth to décollement depicted on published cross sections at 21°S has ranged between 8-11.5 km based on assumptions of the Silurian-lower Devonian thickness (e.g., Baby et al., 1992; Dunn et al., 1995; Kley, 1996; Kley et al., 1999; Moretti et al., 1996; Uba et al., 2009). We assign thicknesses for Silurian rocks based on interpreted seismic reflection data ~65 km along strike to the south (Baby et al., 1992), where the base of the Silurian section is imaged. This places the depth to the basal Silurian décollement at 10 km immediately east of the deformation front, and our depth to decollement approximately splits the variation. We assign a décollement uncertainty of ±0.7 km, the difference between the thicknesses of the Devonian-Silurian section observed at the western edge of the IAZ the thickness we assign in the Chaco Plain. Based on the same logic, we assign a stratigraphic uncertainty of 12% to the eastern edge of the cross-section as 0.7 km is ~12% of the pre-orogenic thickness we assume in the Chaco Plain. Uncertainty of the decollement is reduced to ±500 m across the western SAZ and the IAZ as the Silurian section is exposed and a known thickness for the Silurian rocks can be reasonably assigned in the subsurface.

In the EC, the decollement is interpreted to be located at the basement cover interface, and is imaged by seismic and teleseismic data at ~7-10 km below sea level (Wigger et al., 1994; Schmitz and Kley, 1997; Allmendinger and Zapata, 2000), therefore the depth to decollement for vertices across the EC is assigned a value of ±1.5 km. In the EC, 10-11 km is a reasonable pre-orogenic thickness based on surface observations and geologic mapping. However, the lower part of the Paleozoic section is never exposed in the western EC. Given the variability of for the depth to decollement based on Teleseismic data (±1.5 km), we assign a less optimistic stratigraphic uncertainty of 15% at the western edge of the cross section. Normal subsurface vertices are reasonably well constrained by seismic data tied to well logs, and are assigned uncertainty between 0 and ±500 m, though most vertices in the Chaco Plain have uncertainty between 0 and ± 250 m. Surface vertices are assigned zero uncertainty, assuming that the geologic mapping (Plate 2) is accurate. The majority of vertices are from the eroded hanging walls of thrusts (red dots in Figs. SM7-8). Error on these vertices were assigned based their distance from the surface (Allmendinger and Judge, 2013), ranging from ± 250 m to ± 3.5 km.

The total shortening across the EC, IAZ, and SAZ was calculated using the preferred error estimate for the input parameters discussed in the preceding paragraph (Table SM2, Fig. SM7). The area balance estimate required 2 iterations of calculations (details shown on Table SM2), due to the non-uniform taper of the orogenic wedge (e.g., Allmendinger and Judge, 2013). Total calculated shortening was 259.68 ± 66.8 km, which is comparable to the line length balanced estimate (272 km, Table 1). The uncertainty calculated for the EC to SAZ (68 km) is 24% of the shortening magnitude. We extrapolate this value to the entire retroarc as a whole in order to estimate uncertainty for total shortening, arriving at a value of 337 ± 68.6 km from the Altiplano to the SAZ.

Input parameters were adjusted (only iteration 1) to demonstrate the source of error (Table SM2). As demonstrated by earlier studies (Judge and Allmendinger, 2011; Allmendinger and Judge, 2013), the largest source of error originates from uncertainties pertaining to the stratigraphic thicknesses and depth to decollement (Table SM2). Table SM2 illustrates that errors assigned to eroded hanging wall cutoffs only account for a small amount of the total error.

Area balance estimates of total shortening and uncertainty were also made for the individual tectonomorphic zones (Figs. SM8, SM9, Table SM2). The SAZ estimate does not require the iterative process as the initial wedge for the frontal part of the thrust belt determined from the line length balanced section (Plate 2) is uniformly tapered. The calculated shortening was 82.39 ± 21.57 km, in agreement with the 82 km of shortening calculated from the line length-balanced section (Table 1). Our uncertainty for the SAZ (± 20.57 km) is similar to the uncertainty calculated for the SAZ at 22.5°, 20°, and 19° S (± 15, 17, 15 km respectively) (Judge and Allmendinger, 2011; Eichelberger et al., 2013). Individual estimates from the IAZ and EC were unsuccessful, as the total shortening for the area balance fell well short (>40 km) of the line length balanced estimates. This is likely due to the geometric complexities of the trailing and leading edges of the EC and IAZ (Plate 2), which the simple assumptions of AreaErrorProp cannot resolve (Judge and Allmendinger, 2011). However, because shortening in the IAZ and EC are kinematically linked to progressive emplacement of the same basement thrust sheet, an area balance estimate of shortening and uncertainty were calculated using an enveloping polygon that encompasses both the IAZ and EC (Fig. SM9). The initial wedge of the EC and IAZ had a non-uniform taper; therefore the iterative process was required (Fig. SM8, Table SM3). The total calculated shortening for the IAZ and EC combined was 185.66 ± 45.8 km (Table SM3), comparable to the 190 km of shortening calculated from the line length balanced section (Table 1). The area balance estimates of shortening and uncertainty (Tables SM2-2) are comparable to the line length estimates of shortening (Table 1), and the area balance estimates of shortening and error by individual tectonomorphic zone (Table SM3) are also compatible with the area balance estimate of the thrust belt as a whole (Table SM2). In addition, the shortening error for the SAZ is similar to uncertainty that has been calculated for the SAZ between 22.5° - 19° S. Therefore, the Gaussian errors displayed in Tables SM2 and SM3 are used as the reported errors in the text.

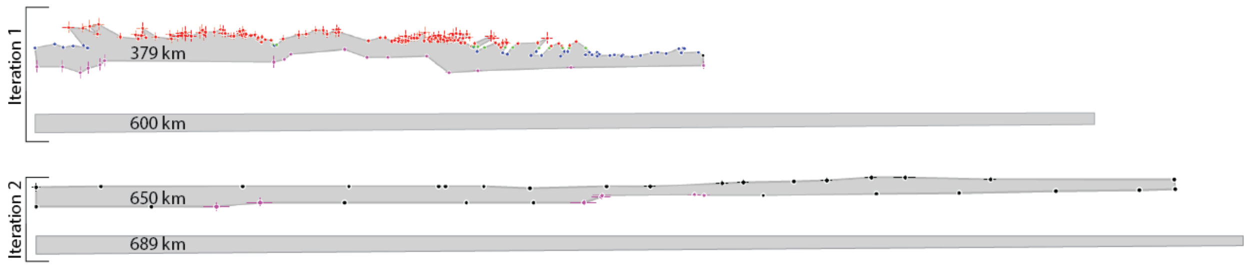

Figure SM7. Area balance of the Andean thrust belt from the EC to the SAZ, showing the two-step iteration for a non-uniformly tapered initial wedge. For each iteration, the enveloping, modern day deformed polygon is shown above and the undeformed initial wedge is shown below. Error bars are displayed on the input parameters, which are color coded as follows: Pink = decollement, blue = normal subsurface vertex, green = surface vertex, red = eroded hanging wall vertex.

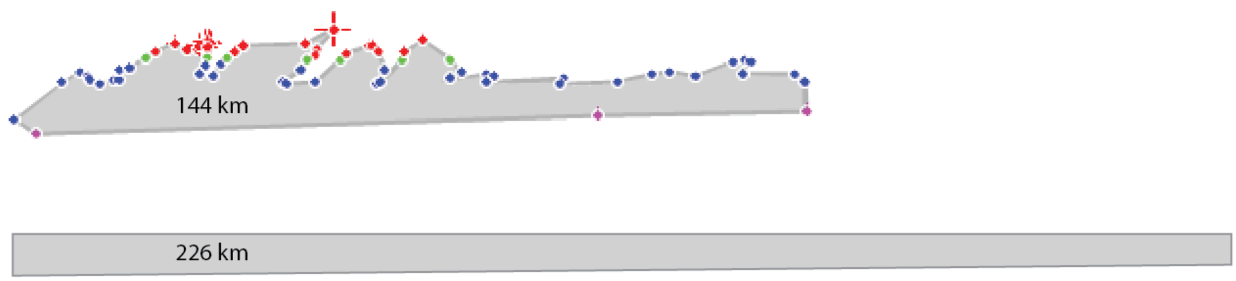

Figure SM8. Area balance of the SAZ. The enveloping, modern day deformed polygon is shown above and the undeformed initial wedge is shown below. Error bars are displayed on the input parameters, which are color coded as follows: Pink = decollement, blue = normal subsurface vertex, green = surface vertex, red = eroded hanging wall vertex.

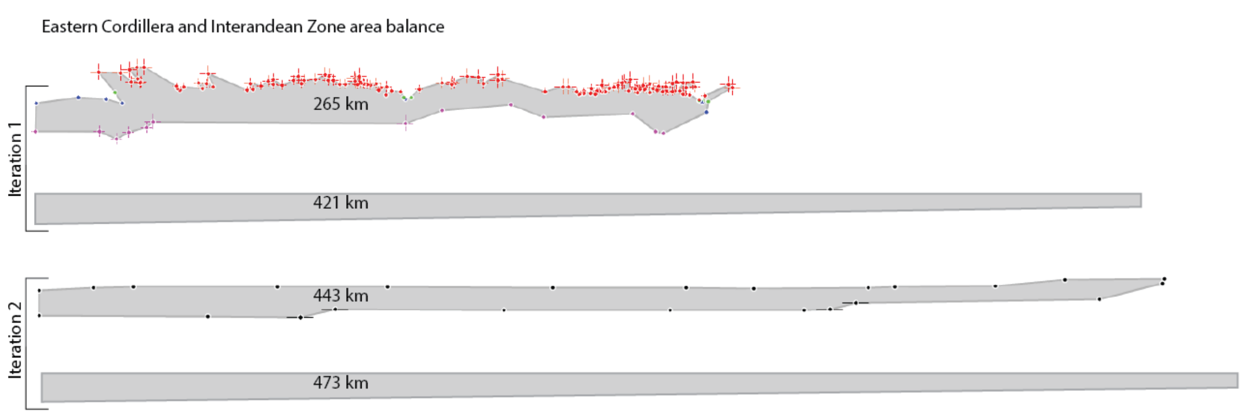

Figure SM9. Area balance of the combined EC and IAZ showing the two-step iteration for a non-uniformly tapered initial wedge. For each iteration, the enveloping, modern day deformed polygon is shown above and the undeformed initial wedge is shown below. Error bars are displayed on the input parameters, which are color coded as follows: Pink = decollement, blue = normal subsurface vertex, green = surface vertex, red = eroded hanging wall vertex.

Table SM2. Area balance estimates of shortening from the EC to SAZ with associated error						
	Shortening (km)	Gaussian error	Maximum error	Shortening (%)	Gaussian error	Maximum error
Preferred uncertainties (iteration 1)	220.57	±66.141	±221.315	±36.78	±6.97	±23.36
No stratigraphic uncertainty	220.57	±18.306	±147.21	36.78	±1.97	±15.58
No decollement uncertainty (iteration 1)	220.57	±64.585	±198	36.78	±6.81	±20.92
No subsurface uncertainty (iteration 1)	220.57	±66.126	±224.118	36.78	±6.97	±23.66
No eroded hanging uncertainty (iteration 1)	220.57	±65.434	±138.827	36.78	±6.90	±9.30
Preferred uncertainties (iteration 2)	-39.11	±9.43	±20.77	5.68	±1.29	±20.77
Total shortening (sum of preferred uncertainties iteration 1 & 2)	**259.68**	**±66.8**		**42.46**	**±7.8**	

Table SM2. Area balance estimates of shortening and uncertainty from the EC to the SAZ. Table displays the total shortening, percent shortening, Gaussian error, and maximum error. Preferred uncertainties are those that are considered based on geologic and geophysical constrains. Changes to input parameters on iteration 1 demonstrate contribution of total error from the different input parameters.

Table SM3. Area balance estimates of shortening by zone with associated error						
	Shortening (km)	Gaussian error	Maximum error	Shortening (%)	Gaussian error	Maximum error
Subandean Zone	**82.39**	**±21.57**	**±61.306**	**36.38**	**±6.06**	**±17.30**
EC and IAZ (iteration 1)	156.27	±45.48	±183.79	37.08	±6.82	±27.79
EC and IAZ (iteration 2)	-29.39	±5.79	±14.02	6.21	±1.15	±2.78
EC and IAZ total (sum iteration 1 and 2)	**185.66**	**±45.8**		**43.29**	**±6.91**	

Table SM3. Area balance estimates of shortening and uncertainty by individual zone. Table displays the total shortening, percent shortening, Gaussian error, and maximum error. Note the EC and IAZ are combined, have a non-uniform initial taper, and require 2 iterations to determine total shortening and uncertainty; whereas, the SAZ does not.

REFERENCES CITED

Allmendinger, R.W., and Judge, P.A., 2013, Stratigraphic uncertainty and errors in shortening from balanced sections in the North American Cordillera: Geological Society of America Bulletin, v. 125, p. 1569–1579, doi: 10.1130/B30871.1.

Allmendinger, R.W., and Zapata, T.R., 2000, The footwall ramp of the Subandean decollement, northernmost Argentina, from extended correlation of seismic reflection data: Tectonophysics, v. 321, p. 37–55, doi: 10.1016/S0040-1951(00)00077-9.

Baby, P., Hérail, G., Salinas, R., and Sempere, T., 1992, Geometry and kinematic evolution of passive roof duplexes deduced from cross section balancing: Example from the foreland thrust system of the southern Bolivian Subandean: Tectonics, v. 11, p. 523–536.

Dunn, J., Hartshorn, K., and Hartshorn, P., 1995, Structural styles and hydrocarbon potential of the Sub-Andean thrust belt of southern Bolivia: .in A.J. Tankard, R. Suarez S., and H.J. Welsink, eds., Petroleum basins of South America: AAPG Memoir 62, p. 523–543.

Eichelberger, N., and McQuarrie, N., 2014, Three-dimensional (3-D) finite strain at the central Andean orocline and implications for grain-scale shortening in orogens: Geological Society of America Bulletin, v. 127, p. 87–112, doi:10.1130/B30968.1.

Eichelberger, N., McQuarrie, N., Ehlers, T. a., Enkelmann, E., Barnes, J.B., and Lease, R.O., 2013, New constraints on the chronology, magnitude, and distribution of deformation within the central Andean orocline: Tectonics, v. 32, p. 1432–1453, doi: 10.1002/tect.20073.

Gubbels, T., Isacks, B., and Farrar, E., 1993, High-level surfaces, plateau uplift, and foreland development, Bolivian central Andes: Geology, v. 21, p. 695–698.

Hérail, G., Oller, J., Baby, P., Bonhomme, M., and Soler, P., 1996, Strike-slip faulting, thrusting and related basins in the Cenozoic evolution of the southern branch of the Bolivian Orocline: Tectonophysics, v. 259, p. 201–212, doi: 10.1016/0040-1951(95)00108-5.

Horton, B.K., 2005, Revised deformation history of the central Andes: Inferences from Cenozoic foredeep and intermontane basins of the Eastern Cordillera, Bolivia: Tectonics, v. 24, p. n/a–n/a, doi: 10.1029/2003TC001619.

Horton, B.K., 1998, Sediment accumulation on top of the Andean orogenic wedge: Oligocene to late Miocene basins of the Eastern Cordillera, southern Bolivia: Geological Society of America Bulletin, v. 110, p. 1174–1192, doi: 10.1130/0016-7606(1998)110<1174:SAOTOT>2.3.CO;2.

Horton, B., 2000, Sediment accumulation on top of the Andean orogenic wedge: Oligocene to late Miocene basins of the Eastern Cordillera, southern Bolivia: Geological Society of America Bulletin, v. 112, p. 1756–1759.

Judge, P.A., and Allmendinger, R.W., 2011, Assessing uncertainties in balanced cross sections: Journal of Structural Geology, v. 33, p. 458–467, doi: 10.1016/j.jsg.2011.01.006.

Kley, J., Monaldi, C.R., and Salfity, J. a., 1999, Along-strike segmentation of the Andean foreland: causes and consequences: Tectonophysics, v. 301, p. 75–94, doi: 10.1016/S0040-1951(98)90223-2.

Kley, J., Muller, J., Tawackoli, S., Jacobshagen, V., and Manutsoglu, E., 1997, Pre-Andean and Andean-Age Deformation in The Eastern: Journal of South American Earth Sciences, v. 10, p. 1–19.

Mitra, S., 1990, Fault-propagation folds: Geometry, kinematic evolution, and hydrocarbon traps: American Association of Petroleum Geologists Bulletin, v. 74, p. 921–945.

Mitra, S., and Namson, J., 1989, Equal-area balancing: American Journal of Science, v. 289, p. 563–599, doi: 10.2475/ajs.289.5.563.

Müller, J.P., Kley, J., and Jacobshagen, V., 2002, Structure and Cenozoic kinematics of the Eastern Cordillera, southern Bolivia (21°S): Tectonics, v. 21, p. 1037, doi: 10.1029/2001TC001340.

Schmitz, M., and Kley, J., 1997, The geometry of the central Andean backarc crust: Joint interpretation of cross section balancing and seismic refraction data: Journal of South American Earth Sciences, v. 10, p. 99–110.

Sempere, T., 2000, Discussion and reply : Sediment accumulation on top of the Andean orogenic wedge: Oligocene to late Miocene basins of the Eastern Cordillera , southern Bolivia: Discussion: Geological Society of America Bulletin, v. 112, p. 1752–1755.

Servicio Geologico de Bolivia, 1992, Mapas Tematicos de Recursos Minerales de Bolivia, Hojas Tarija y Villazon: La Paz, Servicio Geologico de Bolivia, serie II-MTB-1B, scale 1:250,000.

Suppe, J., 1983, Geometry and kinematics of fault-bend folding: American Journal of Science, v. 283, p. 684–721, doi:10.2475/ajs.283.7.684.

Suppe, J., and Medwedeff, D.A., 1990, Geometry and kinematics of fault-propagation folding: Eclogae Geologicae Helvetiae, v. 454, p. 409–454, doi:10.5169/seals-166595.

Tawackoli, S., Jacobshagen, V., Wemmer, K., and Andriessen, P., 1996, The eastern cordillera of southern bolivia: a key region to the Andean backarc uplift and deformation history, in extended abstracts: Third International Symposium on Andean Geodynamics, St. Malo, France. ORSTOM, Paris, p. 505–508.

Uba, C.E., Kley, J., Strecker, M.R., and Schmitt, A.K., 2009, Unsteady evolution of the Bolivian Subandean thrust belt: The role of enhanced erosion and clastic wedge progradation: Earth and Planetary Science Letters, v. 281, p. 134–146, doi: 10.1016/j.epsl.2009.02.010.

Wigger, P., Schmitz, M., Araneda, M., Asch, G., Baldzuhn, S., Giese, P., Heinsohn, W., Martinez, E., Ricaldi, E., Rower, P., and Viramonte, J., 1994, Variation in the crustal structure of the southern Central Andes deduced from seismic refraction investigations: in Tectonics of the Southern Central Andes, edited by K. Reutter et al., Springer- Verlag, New York, 1994., p. 23–48.